Journal of Membrane Science 523 (2017) 205–215

Contents lists available at ScienceDirect

Journal of Membrane Science

journal homepage: www.elsevier.com/locate/memsci

Self-sustained hydrophilic nanofiber thin film composite forward osmosis membranes: Preparation, characterization and application for simulated antibiotic wastewater treatment

Shu-Fang Pan[a,b], Yingchao Dong[a], Yu-Ming. Zheng[a,*], Lu-Bin Zhong[a], Zhi-Hua Yuan[a]

[a] CAS Key Laboratory of Urban Pollutant Conversion, Institute of Urban Environment, Chinese Academy of Sciences, Xiamen 361021, China
[b] College of Resources and Environment, University of Chinese Academy of Sciences, Beijing 100049, China

ARTICLE INFO

Keywords:
Electrospun nanofiber
Forward osmosis
Thin film composite membrane
Antibiotic
Membrane distillation

ABSTRACT

Forward osmosis (FO) is an emerging membrane separation process. However, the lack of high performance FO membrane hinders its wide application. In this study, self-sustained electrospun polyacrylonitrile (PAN) nanofiber supported polyamide (PA) thin film composite (PA/PAN-eTFC) membrane was developed, and evaluated for simulated tetracycline (TC) wastewater treatment. Specifically, a PAN nanofiber support was fabricated by electrospinning without any backing layer. The PAN nanofiber support was then laminated by a paper laminator. The laminated nanofiber support possessed good hydrophilicity and mechanical properties with water contact angle, stress and strain of 32.3 ± 1.3°, 13 ± 0.77 MPa and 68 ± 0.28%, respectively. Polyamide composited membrane formed thereon demonstrated a low structural parameter (S = 168 μm), high permselectivity (A = 1.47 LMH bar^{-1}, B = 0.278 LMH), and achieved over 57 LMH water flux using 2 M NaCl as draw solution. The PA/PAN-eTFC was successfully applied in a forward osmosis–membrane distillation (FO–MD) hybrid process for treatment of simulated TC wastewater and water production for the first time. TC rejection was higher than 99.9%, and 15–22% water recovery was obtained after 7 h running in the FO–MD hybrid process. Meanwhile, the PA/PAN-eTFC membrane exhibited a relatively long-term stable performance in the hybrid system. These results indicate the PA/PAN-eTFC is a promising FO membrane for wastewater treatment.

1. Introduction

Global water scarcity is one of the greatest crises around the world. By 2025, nearly two thirds of the world's population lives in water-deficient area, and millions of people die from waterborne diseases in unsafe water [1,2]. Exploitation of effective and lower-cost methods for water production and water treatment is addressed urgently. As a new membrane process, forward osmosis (FO) has been gaining popularity recently in water production and wastewater treatment [3,4]. FO is a natural process that utilizes an osmotic pressure difference across a semi-permeable membrane to draw water from a dilute solution into a concentrated one [5]. Compared with pressure-driven membrane processes, like reverse osmosis (RO) and nanofiltration (NF), FO possesses some unique advantages such as low energy consumption, low membrane fouling and mild operating conditions [6]. However, FO process has not been applied on a large-scale due to the limit of draw solutions and membrane types. Especially, how to fabricate high-performance FO membranes is a primary obstacle [7,8].

Generally, there are three types of FO membranes: 1) modified NF or RO membranes, 2) asymmetric membranes, and 3) thin film composite membranes (TFC) [6]. Recently, TFC membranes have become more popular because of their superior permselectivity. The active layer and support of TFC membranes can be designed separately, which favors improving the properties of the final TFC membranes. For a high-performance TFC membrane, its active layer should have both excellent permeance and high selectivity. Meanwhile, its support layer must be thin, hydrophilic and highly porous in order to reduce internal concentration polarization (ICP) [9,10]. The ICP usually results in a decrease in both effective osmotic driving force and water flux [11], and it can be indicated by its structural parameter (S). Nevertheless, the TFC membranes, based on the supports fabricated via conventional phase-inversion method, cause severe ICP due to the high S value [10]. So it is very vital to tailor a suitable support layer with a low S for TFC FO membranes.

Multifarious techniques have been studied for the fabrication of a low S value supporting layer for TFC FO membranes, such as

* Corresponding author.
E-mail address: ymzheng@iue.ac.cn (Y.-M. Zheng).

http://dx.doi.org/10.1016/j.memsci.2016.09.045
Received 3 January 2016; Received in revised form 5 September 2016; Accepted 24 September 2016
Available online 04 October 2016

electrospinning [10], co-casting [12] and mixed-matrix membrane fabrication [13], etc. Among membranes that fabricated using the above techniques, the electrospun nanofiber support has demonstrated a very low *S* value due to its scaffold-like structure with interconnected pore, high porosity and large specific surface area [10]. PAN [7], polysulfone (PSf) [14], nylon 6, 6 [15] and polyvinylidene fluoride (PVDF) [16] have been electrospun as nanofiber supports for TFC FO membranes. Though these membranes with low S value possessed high water flux, some of their supports were electrospun from hydrophobic membrane materials such as PSf and PVDF which could weaken the membrane wetting [9]. In addition, the poor mechanical property of electrospun membranes is another obstacle for the large-scale implication of nanofiber-supported membranes. Therefore, it is necessary to explore an electrospun nanofiber support with good mechanical property and hydrophilicity.

In this work, aiming at reducing ICP, we prepared a flat-sheet polyamide TFC membrane (PA/PAN-eTFC) supported by a self-sustained hydrophilic PAN nanofiber. The PAN nanofiber support was first fabricated using an electrospinning process without any backing layer. To reduce overall membrane thickness while obtaining good mechanical strength and hydrophilicity, the nanofiber support was laminated using a paper lamination. Then a polyamide (PA) active layer was polymerized onto the nanofiber support via an interfacial polymerization technique. The structure and performance of both nanofiber support and TFC membrane were characterized in terms of SEM observation, water contact angle measurement, mechanical strength analysis, permeability and permselectity evaluation. Our eTFC membranes were also compared with commercial FO membranes (HTI-CTA and HTI-TFC).

The second objective of this work is to apply the PA/PAN-eTFC membrane for treatment of emerging pollutants in water. Emerging pollutants, including personal care products, disinfection byproducts, and pharmaceuticals, are of increasing concern, which could harm the human health and the ecological security [17]. Antibiotic, a mostly used pharmaceutical for human and livestock, can induce antibiotic resistance genes (ARGs) in waters, which has been attracted widely attention [18,19]. In entry routes of antibiotics, the effluent of pharmaceutical industries is a major part. The antibiotic wastewater generated in manufacturing plants contains high level concentration of antibiotic from around 10–1000 mg/L [20]. So it is urgent to develop a new treatment process for antibiotic wastewater decontamination. Recently, our previous study reported the antibiotic in wastewater can be effectively removed by FO process with a commercial FO membrane [21]. Since the alone FO process cannot produce water, some research groups associated FO process with membrane distillation (MD) process into a FO–MD hybrid system, showing a great potential for water reuse from sewage [22] and oily wastewater [23]. Consequently, a FO–MD hybrid process may be a promising technology for treating tetracycline wastewater to produce fresh water. In this study, the application of FO–MD process for antibiotic wastewater treatment was proposed and studied for the first time. Tetracycline (TC), a widely used broad-spectrum antibiotic, was used to simulate the wastewater. The water flux and TC rejection in FO–MD system was evaluated. Especially, the performance of our TFC FO membranes was investigated.

2. Materials and methods

2.1. Materials and chemicals

Polyacrylonitrile (PAN, M_w = 90000 g/mol) was provided by Kunshan Hongyi Plastic Co. (Suzhou, China). N,N-dimethylformamide (DMF, 99%), N,N-dimethylacetamide (DMAC, 99%) and sodium chloride (NaCl) were obtained from Sinopharm Chemical Reagent Co., Ltd. (Shanghai, China). M-phenylenediamine (MPD, > 99%) and 1,3,5-trimesoyl chloride (TMC, 98%) were purchased from Sigma-Aldrich (St. Louis, MO). Hexane (HPLC, > 99.5%) was supplied by Xiya Reagent (Chengdu, China). Pure tetracycline hydrochloride powder (TC, M_w = 480.90) to simulate antibiotic wastewater was supplied by Beijing Solarbio Science & Technology (Beijing, China). Commercial asymmetric cellulose triacetate (HTI-CTA) and thin film composite membrane (HTI-TFC) FO membranes were acquired from Hydration Technology Innovations Inc. (Albany, OR).

2.2. Membrane preparation

The preparation of nanofiber supported TFC membrane was schematically illustrated in Fig. 1, which was divided into two steps: fabrication of nanofiber support and interfacial polymerization of polyamide layer.

2.2.1. Fabrication of nanofiber support

PAN powder was dissolved in a mixture of DMF and DMAC, and stirred at 60 °C for 5 h to obtain a homogenous solution. The specific experimental conditions of PAN electrospinning were summarized in Table 1. A 9 mL as-prepared spinning solution was directly electrospun onto aluminium foil without any backing layer. The nascent nanofiber mat was peeled off from the aluminium foil and placed into an oven for 12 h to completely volatilize the solvent. Afterwards the mat was sandwiched between two pieces of paper and laminated through a paper laminator (No.3893, Deli, China), resulting in the formation of a stable nanofiber membrane with sufficient mechanical property.

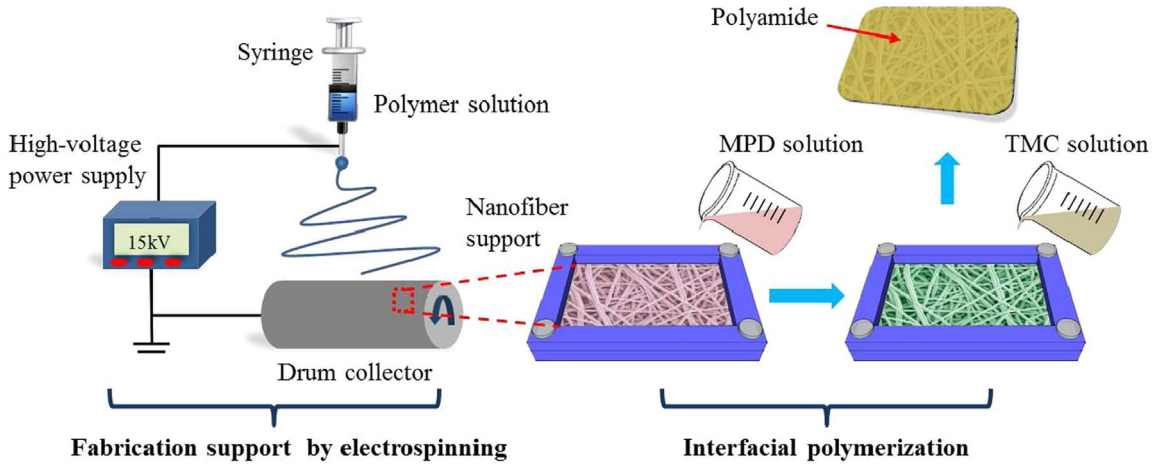

Fig. 1. Schematic diagram of preparation of electrospun nanofiber supported TFC membrane.

Table 1
Experimental conditions of fabrication of PAN nanofiber.

Parameters	Values
Polymer	PAN
Concentration	10%
Solvent	50%DMF: 50%DMAC
Voltage	15 kV
Flow rate	1.2 mL/h
Tip to collector	15 cm
Collector	Aluminium foil

2.2.2. Interfacial polymerization of polyamide layer

A thin polyamide (PA) active layer was deposited on the PAN nanofiber support by interfacial polymerization between MPD and TMC. Briefly, the support membrane was firstly immersed into a 3% (w/v) MPD aqueous solution for 2 min. The membrane was then taken out and excess MPD solution was removed from the membrane surface using tissue papers. Secondly, the nanofiber support was fixed by a dual-tier frame, and then a solution of 0.2% (w/v) TMC in hexane was poured onto the top surface of the support for 1 min to form an ultrathin polyamide film. Finally, the freshly prepared TFC membrane was cured in a vacuum oven at 80 °C for 10 min and then stored in DI water at 4 °C for 24 h.

2.3. Characterizations of PAN nanofiber support and PA/PAN-eTFC FO membrane

The surface morphologies of membranes were acquired with a field emission scanning electron microscope (FESEM, S-4800, Hitachi, Japan). For cross-sectional imaging, the PA/PAN-eTFC membrane was frozen in liquid nitrogen and subsequently cracked to obtain a clean edge. To obtain better contrast and to avoid charge accumulation, samples were sputter coated with a thin layer of gold before imaging. The images were captured with an accelerating voltage of 5 kV. Diameter distribution of fibers was determined by randomly measuring 60 different fibers.

Water contact angles on the nanofiber support surface were characterized by a sessile drop method using a contact angle analyzer (DSA 100, KRUSS, Germany). The volume of tiny droplet was fixed at 5 μL and the values were taken at 0 s, 1 s and 10 s after the water drop deposited on the surface.

The mechanical properties of the as-prepared nanofiber support membranes were evaluated by a tensile test using a universal tensile machine (AGS-X, Shimadzu, Japan). Before tests, the support membranes were tailored into the strips with a dimension of 2.7 cm × 7 cm. A span length of 5 cm and a crosshead speed of 30 mm/min were employed for all the tests which were conducted in triplicate. Thickness of the membranes was measured using a digital micrometer.

The functional groups of PA/PAN-eTFC membranes were characterized under transmission infrared using Fourier transform infrared spectroscopy (FTIR, iS10, Thermo, USA). The scan wave was over the range of 400–4000 cm^{-1} and the number of scan was 16.

2.4. Forward osmosis tests

A lab-scale FO system was employed to evaluate the performance of FO membranes. A custom-made membrane cell with an effective dimension of 100 mm × 40 mm × 2 mm was utilized, in which the crossflow velocity of both solutions was fixed at 12.5 cm/s (600 mL/min) using peristaltic pumps (WT600, Longer, China). The temperature of the feed and draw solutions was kept at 25 °C. For the test against time, the initial volumes of draw and feed solutions were fixed at 2 L. The feed solution was successively stirred to keep its homogeneity. In order to determine the water flux, weight changes of draw solution were recorded automatically every 1 min using a digital balance (SF6001F, Ohaus, USA) connected to a computer. In addition, the conductivity of feed solution was monitored using a conductivity meter (CON110, Eutech Instruments, Singapore) for determination of reverse salt flux.

The water flux (Jw, $Lm^{-2}\,h^{-1}$, abbreviated as LMH) was determined as follows:

$$Jw = \frac{\Delta V}{a\Delta t} \tag{1}$$

where ΔV (L) is the volume of permeation water collected in a predetermined time Δt (h) during the test, and a is the effective membrane surface (m^2).

Reverse salt flux (Js, $gm^{-2}\,h^{-1}$, abbreviated as gMH) was calculated by the following equation:

$$Js = \frac{c_F V_F - c_{F,i} V_{F,i}}{a\Delta t} \tag{2}$$

where c_F (mg/L) and V_F (L) refer to the salt concentration and total volume of the feed at the end of tests, respectively, while $c_{F,i}$ (mg/L) and $V_{F,}i$ (L) are the initial salt concentration and total volume at the beginning of tests.

2.5. Determination of transport and structural parameters

The methodology developed by Tiraferri et al. [24] was used to determine the water permeability coefficient (A), salt permeability coefficient (B) and structural parameter (S) of PA/PAN-eTFC FO membrane. Briefly, the FO test was divided into four stages and each stage was supplied with a different concentration of draw solution. The experimental water and reverse salt fluxes in each stage were fitted by performing a least-squares non-linear regression, determining A, B and S. This fitting based FO transport equations were shown as follows:

$$Jw = A\left\{\frac{\pi_D \exp(-\frac{JwS}{D}) - \pi_F \exp(\frac{Jw}{k})}{1 + \frac{B}{Jw}[\exp(\frac{Jw}{k}) - \exp(-\frac{JwS}{D})]}\right\} \tag{3}$$

$$Js = B\left\{\frac{c_D \exp(-\frac{JwS}{D}) - c_F \exp(\frac{Jw}{k})}{1 + \frac{B}{Jw}[\exp(\frac{Jw}{k}) - \exp(-\frac{JwS}{D})]}\right\} \tag{4}$$

where c_D (mg/L) is the draw solution concentration, and π_F (bar) and π_D (bar) are the osmotic pressures respectively corresponding to the feed solution and draw solution. D is the bulk diffusion coefficient of the draw salt, while k is the mass transfer coefficient of the feed solute. This methodology was embedded in the algorithms by imposing $k \to \infty$.

Meanwhile, the structural parameter (S) is also defined as follows:

$$S = \frac{t\tau}{\varepsilon} \tag{5}$$

where t, τ and ε are the support thickness, tortuosity and porosity, respectively.

It is recommended that the coefficient of variation (CV) of Jw/Js in four stages should be less than 10% and R^2 for both water and salt fluxes should be higher than 0.95. In this work, 0.3 M, 0.5 M, 1.0 M and 2.0 M NaCl solutions were employed as draw solution in four stages of the experiment in FO mode and DI water was used as feed solution for all the tests.

2.6. FO–MD system for TC wastewater treatment

A lab-scale FO-MD system employed for TC wastewater treatment is displayed in Fig. 2. The part of FO setup is the same as that described in Section 2.4. A direct contact MD membrane cell with an effective dimension of 100 mm × 40 mm × 10 mm was used. In the FO–MD hybrid system, the draw solution reservoir of the FO unit was also the feed reservoir for the MD unit, and in order to facilitate the formulation, this solution was referred to as draw solution. The peristaltic

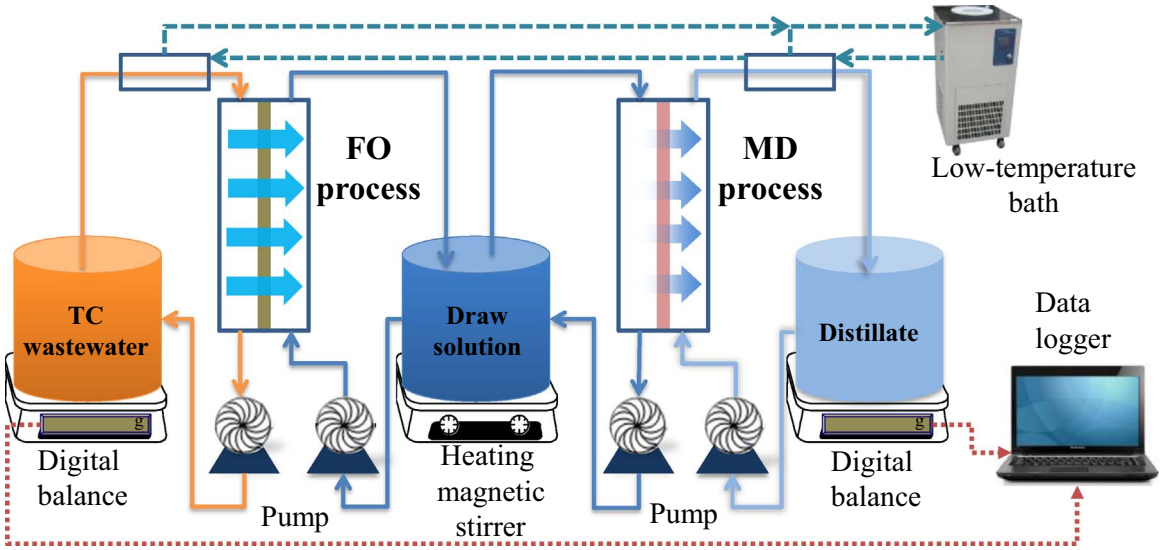

Fig. 2. Schematic diagram of forward osmosis (FO) - membrane distillation (MD) hybrid system..

pumps were employed to circulate the draw and distillate solutions at a cross-flow velocity of 1.67 cm/s (400 mL/min) in MD process, while the velocity of the draw and TC solutions in FO process was 12.5 cm/s (700 mL/min). The TC and distillate solutions were respectively kept at 25 °C and 20 °C using a low-temperature water bath (DHGF-2005, Great Wall, Zhengzhou, China), while the draw solution was maintained at 70 °C in a heating stirrer. In addition, transmembrane temperature difference was measured by a multi-channel temperature monitor in both sides of MD cell. Weight changes of the draw and distillate solutions were recorded automatically every 1 min by digital balances. Conductivity meters were used to monitor the conductivity changes of the feed and distillate solutions.

A hydrophobic microporous membrane used for the MD process was supplied by our lab. The flat MD membrane was fabricated using poly (vinylidene fluoride) (PVDF), exhibiting a thickness of 98.7 μm and a water contact angle of 135°.

2.7. Characterizations of water flux, TC rejection and water recovery

To characterize the water flux, TC rejection and water recovery in the FO–MD system, 2 L TC feed solution, 1 L NaCl draw solution (0.6 M) and 1 L DI distillate water were used. The water flux in MD unit was determined according to Eq. (1). The TC concentrations in the feed solution, draw solution and distillate water were measured using an ultraviolet spectrometer (UV, T-18, P general, China) at the initial and end of tests. The TC rejection in FO process and FO–MD process can be calculated from the following equations:

$$\text{Rejection}=\left(1-\frac{c_{p-draw}}{c_{F,i}}\right)\times 100\% \quad \text{(in FO process)} \tag{7}$$

$$\text{Rejection}=\left(1-\frac{c_{p-distillate}}{c_{F,i}}\right)\times 100\% \quad \text{(in FO–MD system)} \tag{8}$$

where $C_{F,}i$ (mg/L) is the initial TC concentration in the feed solution. $c_{p\text{-}draw}$ (mg/L) is the TC concentration of FO-induced permeate in draw solution and $c_{p\text{-}distillate}$ refers to TC concentration of the permeate in distillate solution. Notably, unlike the conventional pressure-driven process, the TC concentration of permeates were obtained from the difference between TC initial and final concentrations in the draw solution and in the distillate solution. As a result, the $c_{p\text{-}draw}$ and $c_{p\text{-}distillate}$ can be determined using the following equation:

$$c_{p-draw}=\frac{c_D(V_{D,i}+\Delta V_D)-c_{D,i}V_{D,i}}{\Delta V_D} \tag{9}$$

$$c_{p-distillate}=\frac{c_{Dis}(V_{Dis,i}+\Delta V_{Dis})-c_{Dis,i}V_{Dis,i}}{\Delta V_{Dis}} \tag{10}$$

Where c_D (mg/L) and c_{Dis} (mg/L) are the TC concentration in the draw solution and in the distillate solution, respectively. $c_{D,\,i}$ (mg/L) and $c_{Dis,\,i}$ (mg/L) refer to the TC concentration of initial draw solution and distillate solution. The initial volumes of the draw and distillate solutions are expressed as $V_{D,}i$ (L) and $V_{dis,i}$ (L) respectively and the changes of the draw and distillate solutions are ΔV_D (L) and ΔV_{Dis} (L), respectively.

The feed water recovery was calculated according to the equation shown as follows:

$$\text{Recovery}=\left(1-\frac{\Delta V_{Dis}}{V_{F,i}}\right)\times 100\% \tag{11}$$

3. Results and discussion

3.1. Characterization of PAN nanofiber support

The nascent nanofiber support was rough and fluffy, leading to an inconvenience for interfacial polymerization of polyamide layer. In order to improve the hydrophilicity and mechanical property, the electrospun PAN nanofiber support was laminated using a paper laminator. The morphology and hydrophilicity of the PAN nanofiber support are shown in Fig. 3. Compared with the nascent one, the nanofiber support became more smooth and tighter after laminating (Fig. 3a). A representative SEM image of nanofiber support is exhibited in Fig. 3b, the insert of which shows a statistical diameter size distribution of the nanofibers. The bead-free and uniform nanofibers with an average diameter of 502 ± 39 nm were produced. The dynamic contact angle of the PAN nanofiber membrane surface, as exhibited in Figs. 3ci-ciii, decreases to 32.3 ± 1.3° after 1 s from an initial value of 54.8 ± 1.8°, ultimately reaching 0° after ~10 s. This rapid absorption of water droplet on the surface showed a high hydrophilicity which could favor water transport and therefore improve antifouling property [25,26]. The hydrophilicity of the electrospun nanofibers used as TFC-FO supports in previous studies was tabulated as shown in Table 2. Compared with other hydrophilic fibers such as PVA [27] and PA [15], the PAN fibers has comparable contact angle. Interestingly, our

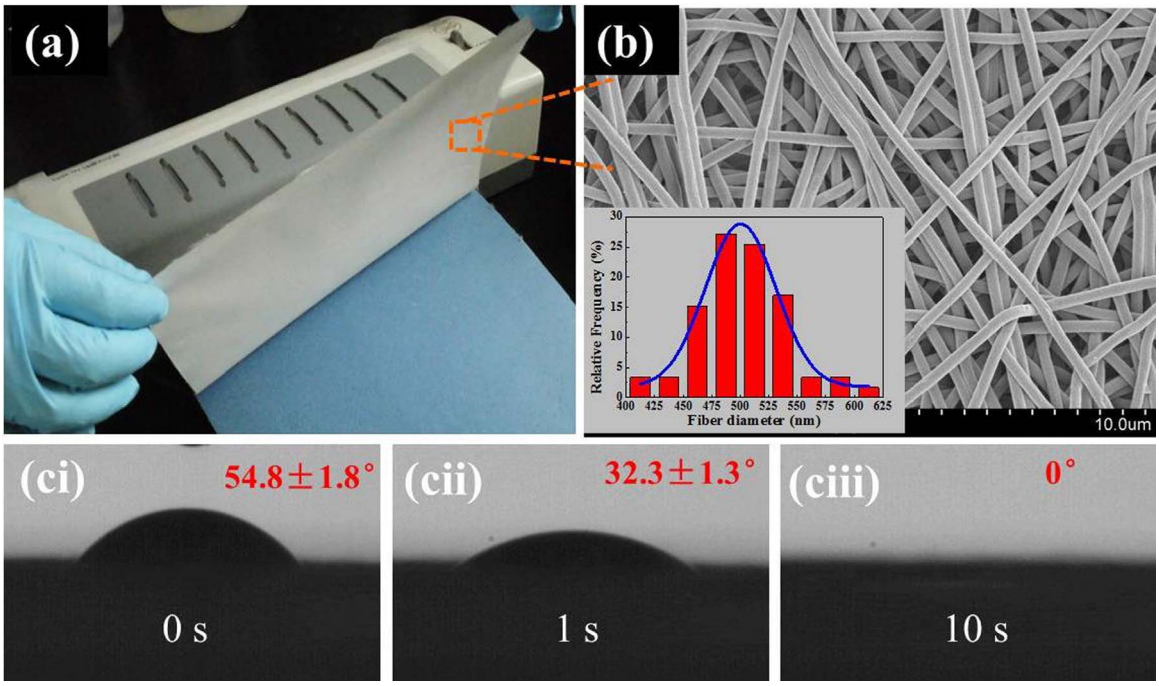

Fig. 3. (a) Photograph, (b) FESEM image and (ci-ciii) dynamic water contact angles of laminated PAN nanofiber support. The inserted figure (bottom left, figure b) shows a statistical diameter size distribution of the nanofibers.

Table 2
The hydrophilicity and mechanical properties of the electrospun nanofibers support.

Support materials	Post-treated method	Contact angle (°)	Stress at break (Mpa)	Elongation at break (%)	Ref.
PAN	Laminating	32.3 ± 1.3	13 ± 0.77	68 ± 0.28	This work
PAN	Isopar treated	69.86 ± 15.83	3[a]	80[a]	[7]
20CA/PAN	Isopar treated	89.28 ± 4.52	2[a]	25[a]	[7]
PAN	Hot-press and PVA coating	–	9 ± 3	20 ± 5	[30]
SiO_2/PAN	Hot-press and PVA coating	–	17 ± 2	15 ± 5	[30]
PVA	Glutaraldehyde Crosslinked	52.48 ± 3.3	5.2[a]	12[a]	[27]
PVDF-1	Heat-press	137.8 ± 2.1	11.1 ± 1.2	37.1 ± 12.0	[16]
PVDF-2	Heat-press	135.8 ± 2.4	11.9 ± 1.9	40.2 ± 4.9	[16]
PA 6,6	–	38 ± 4	10	–	[15]

[a] Values estimated from graphs.

laminated PAN nanofiber support is more hydrophilic than the isopar-treated one [7], considering the laminated support is smoother and thus possessing less microscopic bumps on the surface. The surface hydrophilicity is determined by the polymer hydrophilicity and micro-structure of nanofiber support surface. When the polymer is the same, the rougher surface and hierarchically structured can reduce the surface hydrophilicity [28]. As for the PAN nanofiber support without compaction, the nanofibers hanging on the top surface formed nano protrusions and increased the surface fractions of air and water, resulting in the higher contact angle [29]. The laminating process made the hanging fibers cling to surface, which reduced the nano protrusions and improved the surface hydrophilicity. Additionally, in order to observe the change of hydrophilicity intuitively, water spreading and transport abilities of our lab-made nascent and laminated nanofiber support were compared in a short video (Video. S1). When the water dropped on the nascent support, the water droplet can stand on the surface, while the water droplet on the laminated support spread rapidly on the surface (Fig. S1). So in order to assist water adhesion, the surface of support should be smooth..

Supplementary material related to this article can be found online at http://dx.doi.org/10.1016/j.memsci.2016.09.045.

Electrospun nanofiber membranes were considered to have poor mechanical strength, which was ascribed to a weak bonding between the individual nanofibers. So in order to improve the mechanical properties, as seen in Table 2, some post-treated methods, such as heat-pressing and cross-linking, were often used. The mechanical properties of nanofiber supports are also listed for comparison in Table 2. The stress and elongation at fracture for the laminated PAN nanofiber support in this work were 13.0 ± 0.8 MPa and 68 ± 0.28%, respectively, and the stress-strain curve is shown in Fig. S1. On the premise of making a comprehensive consideration of stress and elongation, it was noted that our laminated PAN membrane has superior strength compared to other nanofibers such as PVA [27] and PVDF [16]. After the laminating process, the cross between random distribution fibers became tighter, demonstrating a compacted non-woven fabric structure (Fig. 3b). When the tension was applied, the force on individual fiber was less due to the larger number of fibers in unit volume, and further, the friction force between fibers increased, which contributed to the better strength property. Meanwhile, the tight fibers still maintained the same high flexibility as the original fibers. The relatively high hydrophilicity, flexibility, and strength of PAN nanofiber membrane made it desirable as a TFC-FO membrane support.

3.2. Characterization of PA/PAN-eTFC membrane

In our study, a complete PA/PAN-eTFC membrane was comprised of a PAN nanofiber support and an active PA layer, without using any backing layer such as polypropylene (PP) or polyester (PET). The total thickness of a PA/PAN-eTFC was estimated to be 80 ± 4 μm as measured using a micrometer. Fig. 4a and b exhibit the photograph and SEM image of cross-sectional structure of the PA/PAN-eTFC, respectively. As shown in Fig. 4b, the nanofiber support has a unique scaffold-like structure, which has interconnected pores between individual nanofibers. In contrast to the conventional supports made via phase-inversion method, such scaffold-like structure could facilitate a better mass transfer in FO process [10,30]. It also can be seen that a PA active layer was integratedly bonded with nanofibers on the top of the support, indicating a strong bonding between PA active layer and its nanofiber support.

In Figs. 4c and d, the surface of thin PA active layer and the bottom layer of PA/PAN-eTFC were imaged by high-resolution SEM. The top view of PA layer (Fig. 4c) exhibits a typical ridge-and-valley morphology, which was formed via interfacial polymerization [31]. The bottom layer of PA/PAN-eTFC, as shown in Fig. 4d, indicates that the morphology of the support was not affected during interfacial polymerization except for a thin PA layer deposited on the top. Furthermore, to confirm the formation of an active layer on the PAN nanofiber support, the PA/PAN-eTFC and the PAN nanofiber support were characterized by FTIR (Fig. 5). From the figure, the formation of a PA active layer was further substantially evidenced by the presence of some additional absorption peaks in the FTIR spectrum of PA/PAN-eTFC, as compared to that of the PAN support. The absorption peaks at 1540 cm^{-1} and 1663 cm^{-1} correspond to the groups of –N–H (amide II peak) and –C=O (amide I peak), respectively. Moreover, the aromatic ring breathing of the PA layer is indicated by an absorption peak at 1611 cm^{-1} [32,33].

3.3. FO performance of PA/PAN-eTFC membrane

3.3.1. Permselectivity of PA active layer and structural parameter

The water permeability coefficient (A), salt permeability coefficient (B) and structural parameter (S) of the PA/PAN-eTFC membrane were evaluated in FO mode by using the methodology developed by Tiraferri et al. [24]. The values of A, B, S, R^2-Jw (correlation coefficient of

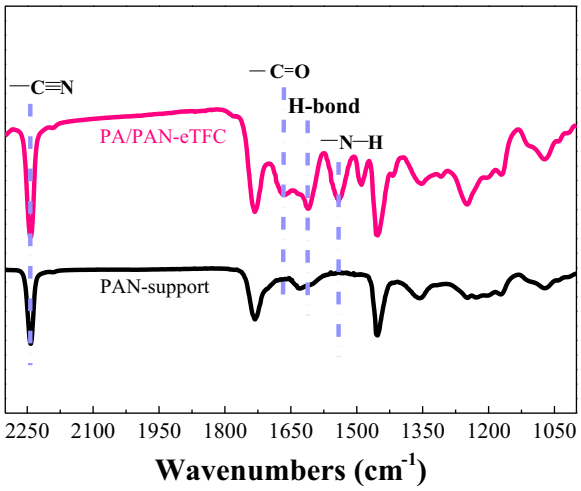

Fig. 5. FTIR spectra of the PA/PAN-eTFC membrane and the PAN nanofiber support.

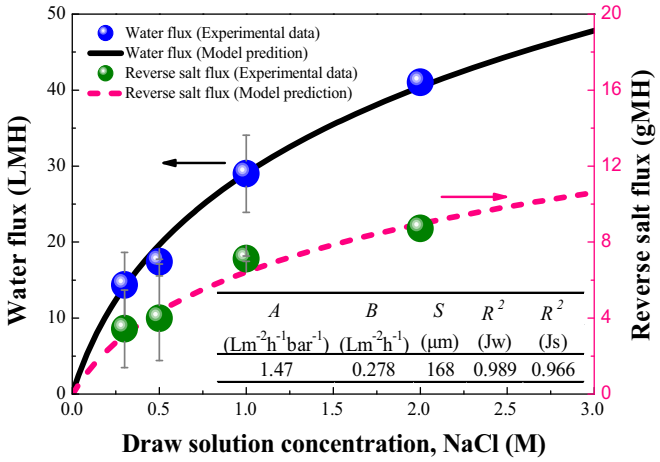

Fig. 6. Experimental data and model prediction of water flux and reverse salt flux of the PA/PAN-eTFC membrane. The inserted table was obtained by using the method developed in Ref. [24]. The model prediction of Jw and Js were obtained by using Eqs. (3) and (4) with the parameters in the inserted table. Experimental conditions: FO mode (active layer facing feed solution), feed solution (DI water), cross-flow velocity (12.5 cm/s), temperature (25 °C).

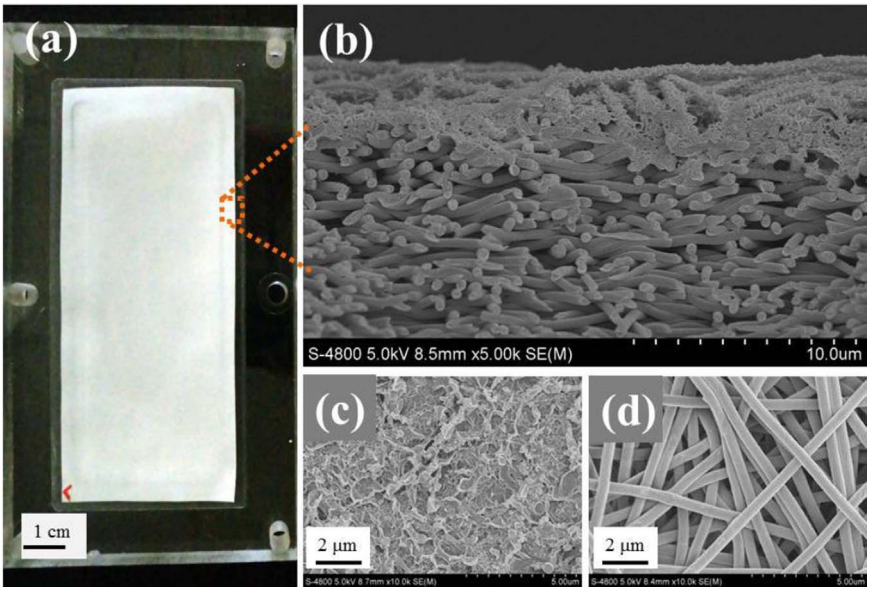

Fig. 4. (a) Optical photograph, (b) cross-sectional SEM image, (c) top PA surface SEM image, and (d) bottom support surface SEM image of the eTFC FO membrane.

determination for the water flux) and R^2-*Js* (correlation coefficient of determination for the salt flux) in the excel-based algorithm were tabulated in Fig. 6, showing a high permselectivity. The model prediction of water flux and reverse salt flux were obtained using the Eqs. (3) and (4) with the parameters of *A*, *B* and *S* in the inserted table in Fig. 6. As shown, the predicted models of *Jw* and *Js* present a good consistence with the experimental data. Under FO mode, the water flux of PA/PAN-eTFC membrane could achieve over 41 LMH using 2 M NaCl as draw solution, and the reverse salt flux maintained below 8.7 gMH.

Nevertheless, it can be found that reverse salt flux of the PA/PAN-eTFC membrane is not very low as shown in Fig. 6. However, it is noteworthy that specific salt flux of the PA/PAN-eTFC is lower than that of the commercial HTI-CTA membrane used in this study, which will be discussed in more detail later. The higher salt flux may be due to the influence of support's hydrophilicity-hydrophobicity on the interfacial polymerization and microstructure of polyamide active layer, thereby affecting the performance of membrane [34,35]. The extent of crosslinking of PA depends on the diffusion of MPD into the interaction zone. The more hydrophilic the support is, the more MPD solution can easily diffuse into pores of the support. Meanwhile the hydrophilic support likely made MPD diffuse slowly out of the pores and into the reaction zone [36], which led to more polyamide formed deep inside the pores of support. So a more hydrophilic support can improve the binding between the polyamide active layer and the support, which was also observed in the PA/PAN-eTFC (Fig. 4). When the amount of polyamide is formed as the same as the thin layer formed with a more hydrophobic support, the thicker film caused by the hydrophilic

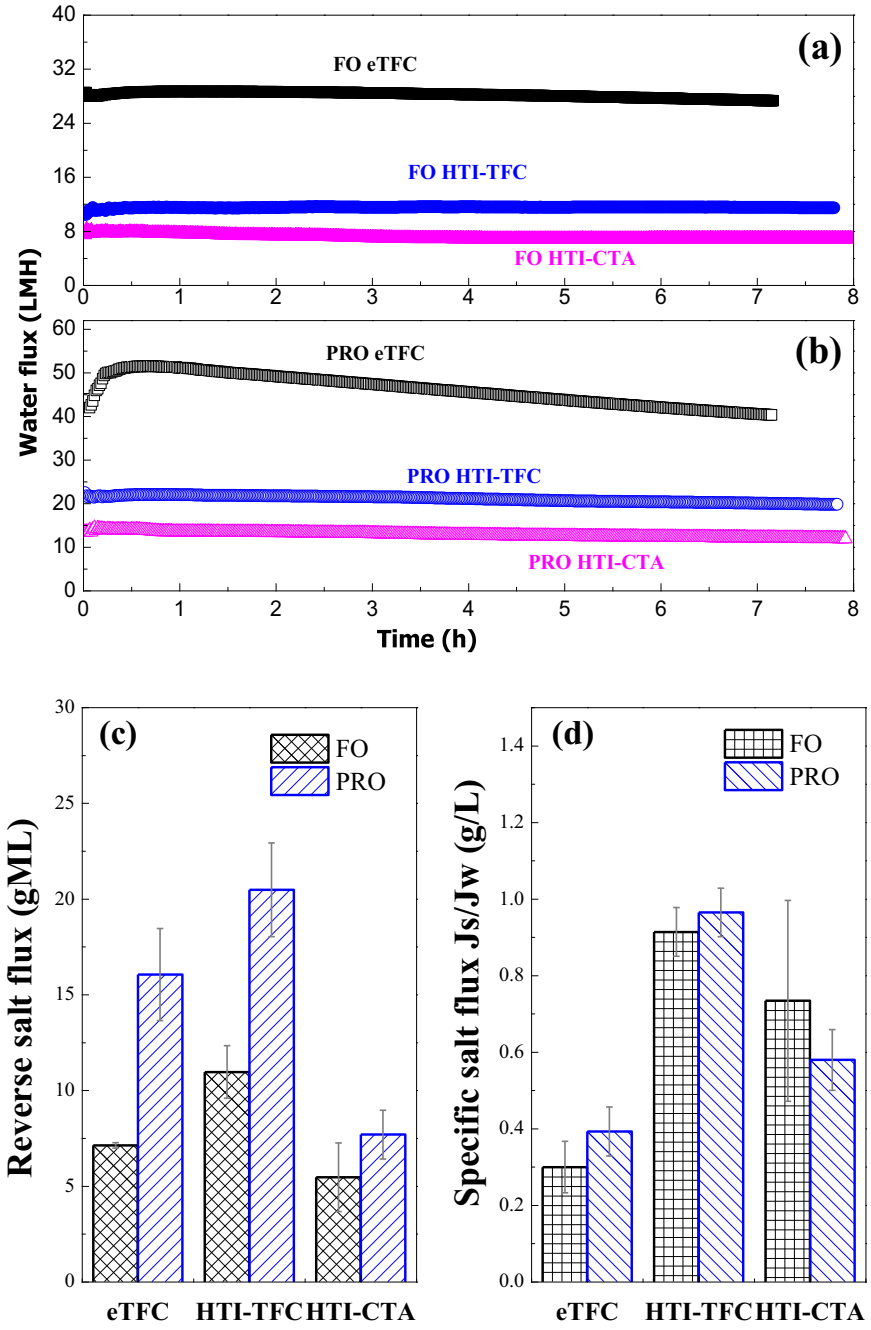

Fig. 7. The performance of PA/PAN-eTFC and commercial FO membranes in osmotic flux tests: water flux in (a) FO mode and (b) PRO mode, (c) reverse salt flux, and (d) specific salt flux. Experimental conditions: DI water as the feed solution; 1.0 M NaCl as draw solution; cross-flow velocities of 12.5 cm/s; 25 °C; FO mode: active layer facing feed solution; PRO mode: active layer facing draw solution.

support was less dense and crosslinking [35], and this can result in a higher reverse salt flux.

It is worth noting that the *S* of PA/PAN-eTFC was 168 μm, which was employed to indicate ICP directly [10]. The higher *S* value is, the more severe ICP appears. Meanwhile, *S* is as a function of thickness (*t*), tortuosity (*τ*) and porosity (*ε*) of the porous nanofiber support according to the Eq. (5), as shown above. ICP developed in the porous supports can be divided into two types: dilutive ICP in FO (active layer facing feed solution) and concentrative ICP in PRO (active layer facing draw solution) [6]. The ICP led to a reduction of the effective osmotic pressure difference ($\Delta\pi_{eff}$) across the membrane, thereby decreasing the water flux. By comparison with some previous studies [37], it is found that the *S* value (168 μm) for our PA/PAN-eTFC was much lower than that (1036 μm) of the phase-inversion-derived TFCs like HTI-TFC. The scaffold-like structure of the PAN nanofiber support possessing low tortuosity (τ) and high porosity (*ε*) is beneficial to salt transport, while the phase-inversion support with a sponge-like structure has a high tortuosity, inhibiting salt diffusion across it [10].

In additional, the *S* of PA/PAN-eTFC in this work is also lower than those of some eTFCs such as 20CA/PAN-TFC (311.1 μm) and PVDF-TFC (325 μm) [7,16], which was attributed to the higher hydrophilicity of our support. The support wetting was very crucial for osmotic flow because the hydrophobicity will significantly reduce the pathways for water transport [9].

3.3.2. Flux of PA/PAN-eTFC membrane

Fig. 7 illustrates behavior and performance of the PA/PAN-eTFC membrane and two commercial FO membranes (HTI-CTA, HTI-TFC) against 1.0 M NaCl. CTA membrane is the earliest commercial FO membrane, belonging to a type of asymmetric membrane, while TFC membrane has attracted more and more attentions due to its superior permselectivity recently. Water flux of all the membranes as a function of testing time in FO and PRO modes are demonstrated in Figs. 7a and b, respectively. It was found that all the membranes in PRO mode show much higher water flux than that in FO mode. This is mainly attributed to that the dilutive ICP in FO mode results in a much lower $\Delta\pi_{eff}$ than that resulted from the concentrative ICP in PRO mode [11]. On the other hand, the water flux of PA/PAN-eTFC membrane maintained stable at least for 7 h in FO mode. However, there is a slight decline in water flux of the PA/PAN-eTFC membrane in PRO mode (Fig. 7b). The major reason for this is that the large water flux diluted the draw solution and then further resulted in a decrease of $\Delta\pi_{eff}$. What's worse the larger water flux would exacerbate the concentrative ICP in PRO mode, thereby resulting in a self-dampening [4].

Compared with HTI-CTA membrane, the PA/PAN-eTFC membranes yielded about 3-fold higher water flux performance in both FO and PRO modes (Figs. 7a and b). This is mainly attributed to a denser structure of the active layer of CTA membranes, which endowed a low water permeability coefficient (0.46 LMH bar^{-1}) [9,37]. On the other hand, the reverse salt flux of PA/PAN-eTFC is 30% and 107% higher than that of CTA membrane in FO mode and PRO modes, respectively (Fig. 7c). However, it is noteworthy that the specific salt flux of PA/PAN-eTFC is 60% and 32% lower than that of CTA in FO and PRO modes, separately (Fig. 7d).

When different membranes and/or experimental conditions were utilized, the specific salt flux was employed to evaluate overall membrane performance, and *Js/Jw* mean loss of draw solute per unit of water produced [38,39]. Lower ratio of *Js/Jw* of the PA/PAN-eTFC reflected an increase in the selectivity of the membrane and higher efficiency of the process [38].

Figs. 7a and b demonstrate that the water flux of PA/PAN-eTFC membrane is 2 times higher than that of HTI-TFC membrane. As reported in the previous study [40], *A* and *B* of HTI-TFC were 1.24 LMH bar^{-1} and 0.37 LMH, respectively. It is found that the PA/PAN-eTFC has only slightly higher water permeability (1.47 LMH bar^{-1}) than that of HTI-TFC. Hence, the lower water flux of the HTI-TFC membrane should be attributed to the much larger *S* (1036 μm) [37]. Such a HTI-TFC membrane was prone to suffer from severe ICP under a high concentration draw solution. The scaffold-like structure of nanofiber support could weaken ICP [10], while the phase-inversion support of HTI-TFC went against the ICP alleviation. The *Js* and *Js/Jw* of HIT-TFC are higher than those of the PA/PAN-eTFC (Figs. 7c and d), which reveals that the PA/PAN-eTFC has a better selectivity.

Along with comparison to commercial FO membranes, our PA/PAN-eTFC membranes were also compared with other membranes reported in the literature, especially for nanofiber supported ones (Table 3). As shown in the Table 3, the PA/PAN-eTFC membrane exhibits much higher water flux than phase-inversion membrane supported TFC. Compare with other nanofiber supported TFC membranes, the PA/PAN-eTFC membrane also demonstrates improved water flux in both FO and RO mode. In terms of specific salt flux, the PA/PAN-eTFC membrane had a much lower value than the phase-inversion membrane supported TFC, which was mainly due to the better salt transportation and lower ICP of nanofiber supports. In general, the PA/PAN-eTFC membrane endows high water flux and low specific salt flux, implying that the PA/PAN-eTFC is a promising membrane for forward osmosis.

3.4. Application of PA/PAN-eTFC FO membrane in FO–MD hybrid process for TC wastewater treatment

3.4.1. Water flux behavior in FO–MD system

Fig. 8a and b display individual water flux of FO and MD process in FO–MD system as a function of time, in which 0.6 M NaCl for simulating seawater at 70 °C was used as draw solution. From Fig. 8a, we can found that baseline (DI water as feed) water flux of PA/PAN-eTFC achieves over 50 LMH, which is even significantly higher than the flux (29.33 LMH) using 1 M NaCl as draw solution at 25 °C (Table 3). The following factors resulted in this flux increase: one is that the osmotic pressure increased at the higher temperature based on the van't Hoff equation; the second one is that the solute resistivity in the support layer decreased due to the increased diffusion coefficient of NaCl and hence the ICP was reduced; and the third one is

Table 3
Performances of lab-made nanofiber and phase-inversion film supported TFC-FO membranes. All membranes were tested using DI water as the feed.

Membrane	Draw solution (NaCl)	Jw (LMH) (FO/PRO)	Js/Jw (g/L) (FO/PRO)	Ref.
Nanofiber supported TFC				
PA/PAN-eTFC	1.0 M	29.33/51.08	0.24/0.33	This work
PVDF-TFC 1#	1.0 M	11.6/30.4	0.30/0.21	[16]
PVDF-TFC 2#	1.0 M	28.0/47.6	0.46/0.45	[16]
Modified PVDF-TFC	1.0 M	22/31	0.17/0.43	[41]
PA6,6-TFC-0.75	1.0 M	21/27	0.24/0.44	[15]
PET-TFC	1.0 M	12.9/-	–	[42]
PAN-TFC	1.5 M	30/52[a]	0.28/0.07[b]	[7]
Modified PVDF-TFC	1.5 M	30/41	0.3/0.47	[41]
Modified PVDF-TFC	2.0 M	35/50[a]	–	[41]
PA/PAN-eTFC	2.0 M	41/57	0.21/0.35	This work
Phase-inversion membrane supported TFC				
PAN-TFC	1.0 M	19.67/-	–	[33]
PA6,6-TFC	1.5 M	21.9/6.0	0.04/0.1	[9]
CTA hollow fiber TFC	2.0 M	26.7/-	0.16[b]/-	[23]

[a] Values estimated from graphs.
[b] Values calculated from the obtained Jw and Js.

that the reduced water viscosity favored its rapid diffusion across the membrane [23]. When 500 mg/L and 1000 mg/L TC solutions were used as the feed respectively, the both water fluxes underwent similar overall trends as a function of time and a relatively faster decline occurred in later flux curve after 4 h operation. Though a mild decline of water flux was found using different TC solutions, the initial fluxes started from about 40 LMH which was around 80% of the value in baseline. It was most likely due to the presence of TC and HCl in the feed solutions, which may be probably illustrated in Fig. 8c. Color of FO membranes became dark against TC solution, indicating that TC was deposited on the membrane surface. The TC-induced membrane fouling led to the pore blocking of the active layer, hence reducing the water flux. Nevertheless, most of similar fouling in FO process could be removed by back washing [8,43].

The water fluxes in MD process are depicted in Fig. 8b, where the transmembrane temperature difference was 43 °C. Unlike the trends in FO process, water flux against 1000 mg/L TC was higher than that against 500 mg/L TC in MD process (Fig. 8b). This may be due to the accumulation of more TC in the draw solution as the higher concentration of TC was used. A MD process in the hybrid system cannot only extract clean water from the simulated antibiotic wastewater, but also recover the draw solution. However, when comparing Fig. 8a with b, we could found that the water flux in FO process is higher than that in MD process. This difference contributed to the continuous dilution of draw

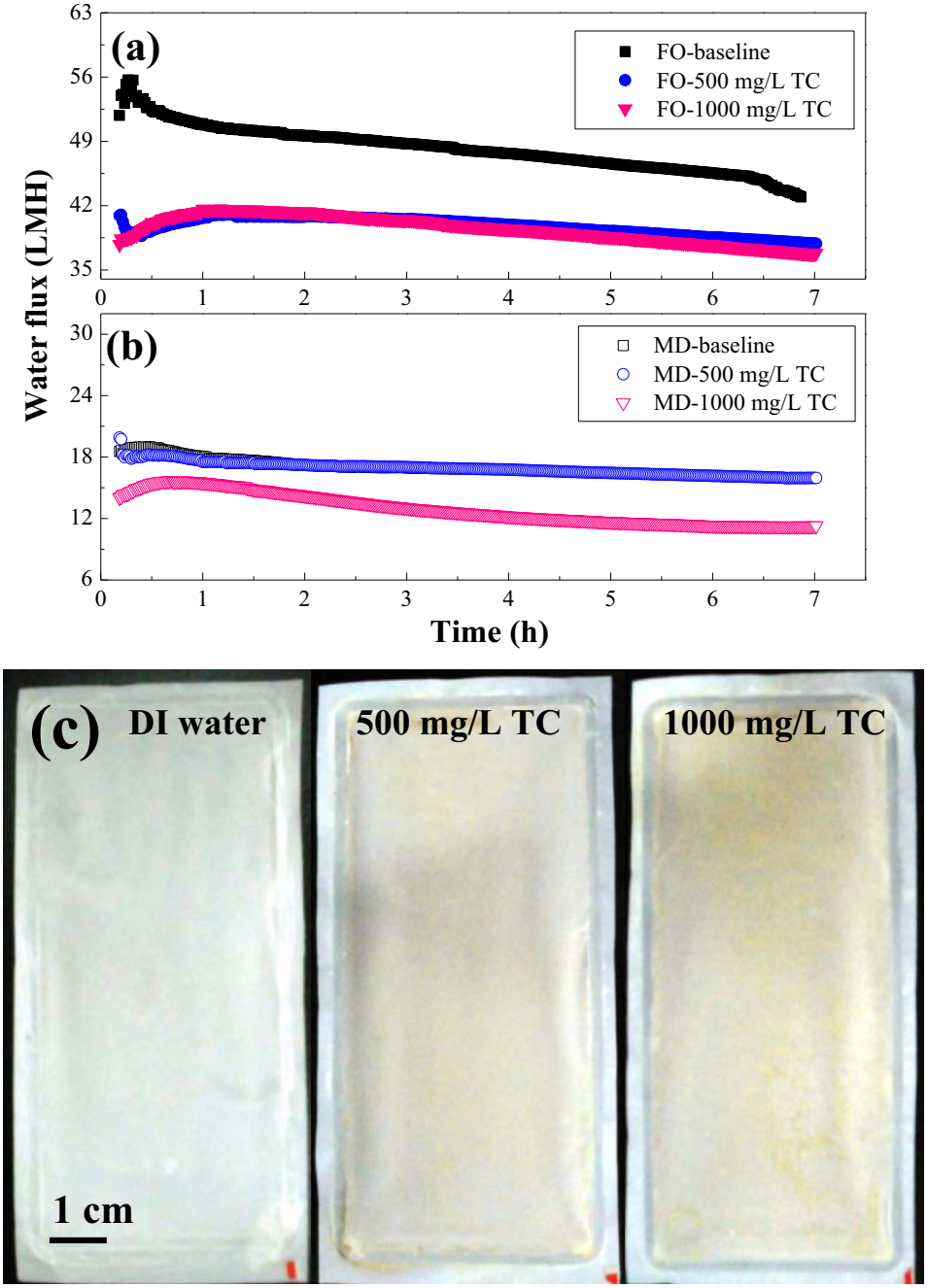

Fig. 8. Water flux in the FO-MD hybrid system for TC treatment: (a) water flux in FO process, (b) water flux in MD process, and (c) The eTFC membrane fouling in FO-MD system for TC wastewater treatment. Experimental conditions: DI water was used as feed solution for baseline; 500 and 1000 mg/L TC solutions were used as feed solution for treatment; 0.6 M NaCl was used as draw solution; the cross-flow velocity of FO unit and MD unit was 12.5 cm/s and 1.67 cm/s, respectively; and temperatures of feed, draw, and distillate solutions were 25, 70, and 20 °C, respectively.

solution and hence decreased the water flux in FO process. As a follow-up of the current work, more experiments such as lowering the concentration of draw solution and increasing the temperature difference, need to be done to keep water flux in the same level.

3.4.2. Removal of TC by FO–MD system

The treatment results of simulated TC wastewater are shown in Fig. 9. The TC concentrations in feed, draw and distillate water of the FO–MD system are presented in Fig. 9a. After 7 h run, TC in feed was enriched about one fold of raw feed by FO process, while accumulation of TC in draw was 0.56 mg/L and 0.75 mg/L using 500 mg/L and 1000 mg/L TC as raw feed, verifying a high rejection of TC solute for the PA/PAN-eTFC membranes. It is noted that the TC content in distillate water was under the detection limit (0.1 mg/L). So the columns of the distillate TC concentration were identified by down arrows in Fig. 9a, which means the values were below 0.1 mg/L. Based on the TC concentrations in feed, draw and distillate, TC rejections calculated from Eqs. (7) and (8) are demonstrated in Fig. 9b. Up arrows present that TC rejection of FO–MD system was over 99.9%, while the rejection in FO process attained 99.8%. In our previous study [21], the commercial HTI-TFC membrane was employed to separate TC from antibiotic wastewater. Compared with HTI-TFC membrane, the PA/PAN-eTFC demonstrates higher TC rejection. The above results reveal that the FO process was an effective pretreatment technology for the subsequent MD process. If the alone MD process was used to treat the wastewater with high content of organics, the PVDF-MD membrane is vulnerable to organic fouling because of its hydrophobicity [22,44].

Fig. 9c shows the water recovery in the hybrid system and the conductivity of distillate water as a function of time. Quantity and quality of the distillate water mainly depended on the MD process on the premise of the removal of most TC by FO process. As seen in Fig. 9c, particularly worth mentioning was that the distillate water endowed a very low conductivity (< 15 μs) which was much lower than tap water with conductivity in the range of 100–200 μs. While about 22% and 15% of feed water were respectively recovered in 500 mg/L and 1000 mg/L TC solutions after 7 h run, which correspond to the MD water flux. As

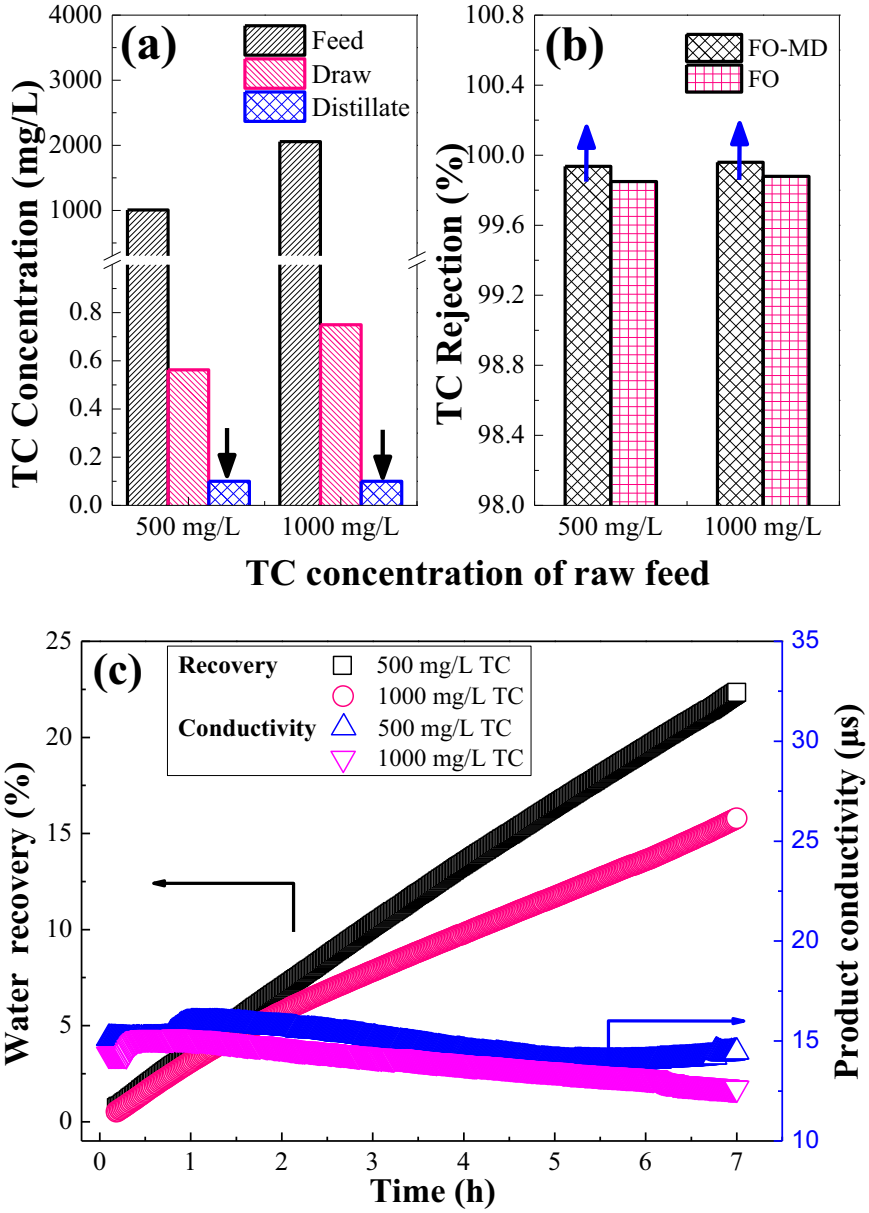

Fig. 9. The treatment performance of TC wastewater by the FO-MD hybrid system. (a) Concentrations of TC in feed, draw and distillate at the end of tests. (b) TC rejections in the FO-MD hybrid system and FO process. The up/down arrows presented the values were higher/lower than that the columns showed. (c) Water recovery of FO-MD system and conductivity of the distillate water. Experimental conditions were the same as those mentioned in Fig. 8.

mentioned above, in order to improve water recovery, the water flux in MD process should be improved. Though the operating conditions of FO–MD system need to be further optimized, the hybrid system with PA/PAN-eTFC membranes could be developed as a promising technology for the treatment of antibiotic wastewater as well as water recovery.

4. Conclusions

In summary, in this study a PA/PAN-eTFC membrane supported by hydrophilic electrospun PAN nanofiber with a scaffold-like structure was fabricated, characterized and applied for TC wastewater treatment via a FO–MD hybrid process. Firstly, the nanofiber support was fabricated by electrospinning without any backing layer. The PAN nanofiber support was then laminated by a paper laminator. The laminated nanofiber support possessed superior hydrophilicity, high flexibility and preferable mechanical strength. Moreover, the nanofiber has a highly porous scaffold-like structure with interconnected pores, allowing a very low S and hence significantly alleviating ICP. Due to high permselectivity and low *S*, the PA/PAN-eTFC membrane exhibited a significantly improved water flux, as compared to commercial FO membranes of HTI-CTA and HTI-TFC. Furthermore, the PA/PAN-eTFC membranes were used in a FO–MD hybrid system for TC wastewater treatment. The results showed the FO–MD hybrid system with PA/PAN-eTFC membranes had an almost complete rejection of TC (with a rejection ratio as high as 99.8%), indicating a great potential for the highly efficient treatment of antibiotic wastewater.

Acknowledgements

This work was funded by the Hundred Talents Program of Chinese Academy of Sciences, the National Natural Science Foundation of China (51578525, 5153000136) and the Xiamen Southern Ocean Research Center (14GQT60HJ30).

Appendix A. Supporting information

Supplementary data associated with this article can be found in the online version at doi:10.1016/j.memsci.2016.09.045.

References

[1] M.A. Montgomery, M. Elimelech, Water and sanitation in developing countries: including health in the equation, Environ. Sci. Technol. 41 (2007) 17–24.
[2] M. Elimelech, W.A. Phillip, The future of seawater desalination: energy, technology, and the environment, Science 333 (2011) 712–717.
[3] B.E. Logan, M. Elimelech, Membrane-based processes for sustainable power generation using water, Nature 488 (2012) 313–319.
[4] J.R. McCutcheon, M. Elimelech, Modeling water flux in forward osmosis: implications for improved membrane design, AlChE J. 53 (2007) 1736–1744.
[5] T.Y. Cath, A.E. Childress, M. Elimelech, Forward osmosis: principles, applications, and recent developments, J. Membr. Sci. 281 (2006) 70–87.
[6] C. Klaysom, T.Y. Cath, T. Depuydt, I.F. Vankelecom, Forward and pressure retarded osmosis: potential solutions for global challenges in energy and water supply, Chem. Soc. Rev. 42 (2013) 6959–6989.
[7] N.N. Bui, J.R. McCutcheon, Hydrophilic nanofibers as new supports for thin film composite membranes for engineered osmosis, Environ. Sci. Technol. 47 (2013) 1761–1769.
[8] P.H. Duong, T.S. Chung, S. Wei, L. Irish, Highly permeable double-skinned forward osmosis membranes for anti-fouling in the emulsified oil-water separation process, Environ. Sci. Technol. 48 (2014) 4537–4545.
[9] J.R. McCutcheon, M. Elimelech, Influence of membrane support layer hydrophobicity on water flux in osmotically driven membrane processes, J. Membr. Sci. 318 (2008) 458–466.
[10] X. Song, Z. Liu, D.D. Sun, Nano gives the answer: breaking the bottleneck of internal concentration polarization with a nanofiber composite forward osmosis membrane for a high water production rate, Adv. Mater. 23 (2011) 3256–3260.
[11] J.R. McCutcheon, M. Elimelech, Influence of concentrative and dilutive internal concentration polarization on flux behavior in forward osmosis, J. Membr. Sci. 284 (2006) 237–247.
[12] P. Xiao, L.D. Nghiem, Y. Yin, X.-M. Li, M. Zhang, G. Chen, J. Song, T. He, A sacrificial-layer approach to fabricate polysulfone support for forward osmosis thin-film composite membranes with reduced internal concentration polarisation, J. Membr. Sci. 481 (2015) 106–114.
[13] W. kuang, Z. Liu, H. Yu, G. Kang, X. Jie, Y. Jin, Y. Cao, Investigation of internal concentration polarization reduction in forward osmosis membrane using nano-$CaCO_3$ particles as sacrificial component, J. Membr. Sci. 497 (2016) 485–493.
[14] N.-N. Bui, M.L. Lind, E.M.V. Hoek, J.R. McCutcheon, Electrospun nanofiber supported thin film composite membranes for engineered osmosis, J. Membr. Sci. 385–386 (2011) 10–19.
[15] L. Huang, J.R. McCutcheon, Hydrophilic nylon 6,6 nanofibers supported thin film composite membranes for engineered osmosis, J. Membr. Sci. 457 (2014) 162–169.
[16] M. Tian, C. Qiu, Y. Liao, S. Chou, R. Wang, Preparation of polyamide thin film composite forward osmosis membranes using electrospun polyvinylidene fluoride (PVDF) nanofibers as substrates, Sep. Purif. Technol. (2013) 727–736.
[17] Ml Farré, S. Pérez, L. Kantiani, D. Barceló, Fate and toxicity of emerging pollutants, their metabolites and transformation products in the aquatic environment, TrAC Trends Anal. Chem. 27 (2008) 991–1007.
[18] X.P. Guo, J. Li, F. Yang, J. Yang, D.Q. Yin, Prevalence of sulfonamide and tetracycline resistance genes in drinking water treatment plants in the Yangtze River Delta, China, Sci. Total Environ. 493 (2014) 626–631.
[19] Y.H. Fei, X.Y. Li, Adsorption of tetracyclines on marine sediment during organic matter diagenesis, Water Sci. Technol. 67 (2013) 2616–2621.
[20] S.F. Pan, M.P. Zhu, J.P. Chen, Z.H. Yuan, L.B. Zhong, Y.M. Zheng, Separation of tetracycline from wastewater using forward osmosis process with thin film composite membrane – Implications for antibiotics recovery, Sep. Purif. Technol. 153 (2015) 76–83.
[21] S.-F. Pan, M.-P. Zhu, J.P. Chen, Z.-H. Yuan, L.-B. Zhong, Y.-M. Zheng, Separation of tetracycline from wastewater using forward osmosis process with thin film composite membrane – Implications for antibiotics recovery, Sep. Purif. Technol. 153 (2015) 76–83.
[22] M. Xie, L.D. Nghiem, W.E. Price, M. Elimelech, A forward osmosis-membrane distillation hybrid process for direct sewer mining: system performance and limitations, Environ. Sci. Technol. 47 (2013) 13486–13493.
[23] S. Zhang, P. Wang, X.Z. Fu, T.S. Chung, Sustainable water recovery from oily wastewater via forward osmosis-membrane distillation (FO-MD), Water Res. 52 (2014) 112–121.
[24] A. Tiraferri, N.Y. Yip, A.P. Straub, S. Romero-Vargas Castrillon, M. Elimelech, A method for the simultaneous determination of transport and structural parameters of forward osmosis membranes, J. Membr. Sci. 444 (2013) 523–538.
[25] P.-C. Chen, L.-S. Wan, Z.-K. Xu, Bio-inspired $CaCO_3$ coating for superhydrophilic hybrid membranes with high water permeability, J. Mater. Chem. 22 (2012) 22727–22733.
[26] L. Liu, B. Shao, F. Yang, Polydopamine coating – surface modification of polyester filter and fouling reduction, Sep. Purif. Technol. 118 (2013) 226–233.
[27] J.M.C. Puguan, H.-S. Kim, K.-J. Lee, H. Kim, Low internal concentration polarization in forward osmosis membranes with hydrophilic crosslinked PVA nanofibers as porous support layer, Desalination 336 (2014) 24–31.
[28] Y. Liao, R. Wang, A.G. Fane, Fabrication of bioinspired composite nanofiber membranes with robust superhydrophobicity for direct contact membrane distillation, Environ. Sci. Technol. 48 (2014) 6335–6341.
[29] L. Yao, J. He, Recent progress in antireflection and self-cleaning technology – from surface engineering to functional surfaces, Prog. Mater. Sci. 61 (2014) 94–143.
[30] X.X. Song, Z.Y. Liu, D.D. Sun, Energy recovery from concentrated seawater brine by thin-film nanofiber composite pressure retarded osmosis membranes with high power density, Energy Environ. Sci. 6 (2013) 1199–1210.
[31] A.K. Ghosh, B.-H. Jeong, X. Huang, E.M.V. Hoek, Impacts of reaction and curing conditions on polyamide composite reverse osmosis membrane properties, J. Membr. Sci. 311 (2008) 34–45.
[32] A. Prakash Rao, S.V. Joshi, J.J. Trivedi, C.V. Devmurari, V.J. Shah, Structure–performance correlation of polyamide thin film composite membranes: effect of coating conditions on film formation, J. Membr. Sci. 211 (2003) 13–24.
[33] P.H.H. Duong, T.S. Chung, Application of thin film composite membranes with forward osmosis technology for the separation of emulsified oil-water, J. Membr. Sci. 457 (2013) 117–126.
[34] M. Fathizadeh, A. Aroujalian, A. Raisi, Effect of lag time in interfacial polymerization on polyamide composite membrane with different hydrophilic sub layers, Desalination 284 (2012) 32–41.
[35] A.K. Ghosh, E.M.V. Hoek, Impacts of support membrane structure and chemistry on polyamide–polysulfone interfacial composite membranes, J. Membr. Sci. 336 (2009) 140–148.
[36] H.I. Kim, S.S. Kim, Plasma treatment of polypropylene and polysulfone supports for thin film composite reverse osmosis membrane, J. Membr. Sci. 286 (2006) 193–201.
[37] D. Stillman, L. Krupp, Y.-H. La, Mesh-reinforced thin film composite membranes for forward osmosis applications: the structure–performance relationship, J. Membr. Sci. 468 (2014) 308–316.
[38] N.T. Hancock, T.Y. Cath, Solute coupled diffusion in osmotically driven membrane processes, Environ. Sci. Technol. 43 (2009) 6769–6775.
[39] W.A. Phillip, J.S. Yong, M. Elimelech, Reverse draw solute permeation in forward osmosis: modeling and experiments, Environ. Sci. Technol. 44 (2010) 5170–5176.
[40] Z.W. Wang, J.X. Tang, C.W. Zhu, Y. Dong, Q.Y. Wang, Z.C. Wu, Chemical cleaning protocols for thin film composite (TFC) polyamide forward osmosis membranes used for municipal wastewater treatment, J. Membr. Sci. 475 (2015) 184–192.
[41] L. Huang, J.T. Arena, J.R. McCutcheon, Surface modified PVDF nanofiber supported thin film composite membranes for forward osmosis, J. Membr. Sci. 499 (2016) 352–360.
[42] L.A. Hoover, J.D. Schiffman, M. Elimelech, Nanofibers in thin-film composite membrane support layers: enabling expanded application of forward and pressure retarded osmosis, Desalination 308 (2013) 73–81.
[43] M. Xie, L.D. Nghiem, W.E. Price, M. Elimelech, Toward resource recovery from wastewater: extraction of phosphorus from digested sludge using a hybrid forward osmosis–membrane distillation process, Environ. Sci. Technol. Lett. 1 (2014) 191–195.
[44] L.D. Tijing, Y.C. Woo, J.-S. Choi, S. Lee, S.-H. Kim, H.K. Shon, Fouling and its control in membrane distillation-a review, J. Membr. Sci. 475 (2015) 215–244.